

Twin Plane Re-entrant Mechanism for Catalytic Nanowire Growth

Andrew D. Gamalski^{1,§}, Peter W. Voorhees^{2,†}, Caterina Ducati³, Renu Sharma⁴,
Stephan Hofmann^{1,*}

¹Department of Engineering, University of Cambridge, Cambridge CB3 0FA, UK

²Materials Science and Engineering, Northwestern University, Evanston, Illinois 60208, USA

³Department of Materials Science and Metallurgy, University of Cambridge, Cambridge CB2 3QZ, UK

⁴Center for Nanoscale Science and Technology, National Institute of Standards and Technology, 100 Bureau Dr., Gaithersburg MD 20899-6203.

Abstract

A twin-plane based nanowire growth mechanism is established using Au catalyzed Ge nanowire growth as a model system. Video-rate lattice-resolved environmental transmission electron microscopy shows a convex, V-shaped liquid catalyst-nanowire growth interface for a $\langle 112 \rangle$ growth direction, that is composed of two Ge $\{111\}$ planes which meet at a twin boundary. Unlike to bulk crystals, the nanowire geometry allows steady state growth with a *single* twin boundary at the nanowire centre. We suggest that the nucleation barrier at the twin-plane re-entrant groove is effectively reduced by the line energy, and hence the twin acts as a preferential nucleation site that dictates the lateral step flow cycle which constitutes nanowire growth.

Keywords: Nanowire, Environmental Transmission Electron Microscopy, Twin Plane Re-entrant Mechanism, Vapor Liquid Solid Growth Model

Corresponding Authors: [†]p-voorhees@northwestern.edu, ^{*}sh315@cam.ac.uk

[§]Current address: Intel Corporation, 5000 W. Chandler Blvd., Chandler, AZ 85226 USA

Twin planes formed during solidification or precipitation are a common defect in a wide variety of materials [1] ranging from semiconductors [2] and Ti-alloys [3], to ceramic materials [4]. Twins are particularly important in crystal growth, where they are known to catalyze crystallization through the twin plane re-entrant mechanism (TPRE) [2, 5-8]. The TPRE mechanism considers reentrant twins as preferential nucleation sites of new atomic layers by which the growth interface progressively advances. In bulk crystals, the presence of two parallel twin boundaries is thereby required for steady-state crystal growth, since a single twin re-entrant groove outgrows itself due to the very low growth rates of $\{111\}$ interfaces [9]. The growth rates of such twinned crystals can readily be on the order of $100 \mu\text{m}/\text{sec}$, indicating that two twins acting in concert can easily provide the nucleation rate required for a highly mobile interface. However, despite the ubiquitous nature of twin defects and the wide acceptance of the need for two twins for steady-state crystal growth, many different models have been proposed for this process and it remains unclear how a twin boundary reduces the barrier for the nucleation of steps, a necessary condition for the TPRE mechanism to operate [4, 9-12].

Here we report the direct observation of twin mediated crystal growth using video-rate lattice-resolved environmental transmission electron microscopy (ETEM). We focus on the Au-catalyzed growth of Ge nanowires (NWs) as model nanoscale system. For $\langle 112 \rangle$ orientated NWs, we find a convex, V-shaped liquid catalyst-nanowire growth interface, composed of two Ge $\{111\}$ planes which connect to the triple-phase boundary via truncated interfaces of high mobility. The NW diameter is much smaller than the typical twin boundary separation observed during classical TPRE, and thus the nanoscale geometry allows steady state growth based on a *single* twin boundary at the NW center. Our data allows us to focus on why a single twin leads to growth and to consistently interpret prior NW literature, e.g. reporting post-growth data of preferential impurity incorporation along twin defects [13, 14] and the frequent observation of twins in NWs growing in the $\langle 112 \rangle$ direction. We propose that the nucleation barrier at the twin plane re-entrant groove is reduced by the presence of a line energy. Our results are of general validity and provide an important insight into the TPRE growth process of bulk materials.

Results

Figure 1 shows bright field ETEM images of a representative Ge NW during growth with a liquid AuGe alloy at its tip. The ETEM images are part of a video sequence [see Supporting Information, Video V1] recorded at 9 frames/s with a modified TEM [15] equipped with a differential pumping system and a digital video camera. The Au catalyst was prepared by thermal evaporation (nominal Au thickness 0.2 nm to 2 nm) onto 2000 mesh Cu TEM grids coated with a holey carbon film and an approximately 30 nm thick sputtered SiO_x or Al_2O_3 layer. We avoid focusing the electron beam on the sample to mitigate electron-beam induced damage, gas dissociation, and modification of the specimen. The Au catalysts were isothermally exposed to either pure digermane (Ge_2H_6), or diluted (30 % mole fraction in He) Ge_2H_6 , or Ge_2H_6 mixed with ammonia (NH_3) at temperatures ranging from ≈ 310 °C to 330 °C. This leads to the formation of metastable liquid AuGe alloy particles from which the Ge NWs nucleate and grow [16, 17].

Figure 1a, c show that during steady growth the Ge NW exhibits a V-shaped convex interface with the liquid AuGe catalyst. Such a convex growth interface geometry has been previously predicted for twinned [14, 18, 19, 20, 21] and non-twinned NWs [22], but to date has not been experimentally observed under growth conditions. Figure 1b schematically highlights the key details of our assignments and the growth interface geometry, based on the analysis of the NW projection for this ETEM video [23] and supported by a systematic analysis of a significant number (>15) of $\langle 112 \rangle$ type Ge NWs [see Supporting Information]. The ETEM data of Figure 1 can be consistently interpreted as showing a $[112]$ orientated Ge NW, imaged slightly off the $[110]$ axis, with a central twin plane running parallel to the electron beam at the NW center. The dark contrast streak running along the twin boundary is likely to be due to Au incorporation [23]. This is consistent with prior literature reporting Au to collect along twin defects in Si NWs [13]. Our ETEM data shows that steady state NW growth is possible based on a *single* twin boundary, in contrast to the two parallel twin boundaries required for stable bulk crystal growth. We use the projected twin boundary of the growing Ge NW as reference direction, as it remains static throughout the ETEM videos.

The liquid AuGe catalyst/Ge interface (Fig. 1) mainly consists of two $\{111\}$ Ge planes at a measured angle ψ of $\approx 131 \pm 2^\circ$, which is consistent with the expected 133° taking into account

the projection. Ge{111} is the slowest growing face with the lowest free energy [24] and thus dominates Ge NW growth. Importantly, the catalyst/NW growth interface is not planar, but notably truncated towards the triple phase boundary (TPB), where the crystalline NW, liquid catalyst and chemical vapor deposition (CVD) atmosphere meet (Fig. 1). Our and other previous work highlighted the lateral step flow cycle that constitutes axial NW growth and the importance of this solid-liquid interfacial morphology near the TPB [16]. For NW growth in the $\langle 111 \rangle$ direction, where a single {111} plane dominates the growth interface, it has been established that the level of TPB truncation directly reflects the catalyst supersaturation and hence shows an oscillatory behavior as NW growth progresses. Each TPB truncation oscillation thereby corresponds to the NW growing by one {111} bilayer [16, 25]. In contrast, Figures 1 c-f show that the highly mobile region of interface near the TPB (schematically highlighted as *i* in Fig. 1b) remains static on a timescale for which the twin region undergoes obvious transformations and the NW growth interface has clearly progressed. This can be rationalized by assuming that a nucleation process at the twin is involved, schematically highlighted as *iii* in Fig. 1b, at a catalyst supersaturation level that is low compared to that of previously reported NW growth in the $\langle 111 \rangle$ direction. Step flow is too rapid to be directly resolved here and experimentally we are limited by the 2D projected nature of the TEM imaging. But our ETEM data indicates that the liquid-solid growth interface advances discretely. Moreover, the convex, V-shaped growth interface geometry with the twin at its center is clearly stable, unlike to bulk crystals, where such convex groove would quickly outgrow itself [9]. Consistent with previous NW literature, we propose that, independent of the detailed crystallography, the high mobility interfaces that connect to the TPB require little supersaturation to move, much less supersaturation than required to nucleate a new layer along the twin boundary (*iii*). Hence the TPB regions advance, as does the whole NW, at a rate completely determined by the nucleation rate at the twin.

The pervasiveness of twinned $\langle 112 \rangle$ oriented nanowires also indicates that twins are required for the growth of these wires. We note that all $\langle 112 \rangle$ orientated Ge NWs of our systematic study exhibited a twin or similar defect along their body. To our knowledge, this is consistent with the entire NW literature, except for very small diameter NWs [26] and very low pressure ($\leq 10^{-4}$ Pa), ultra-high vacuum based exposures. For the latter, NWs have been observed to grow (at very slow rate) ‘sideways’ in the $\langle 112 \rangle$ direction with a single {111} dominated catalyst interface, which is not observed in our experiments since we employ the much higher

exposure pressures commonly used in most experiments. Thus, given that at the conditions used twin nucleation is feasible [18], the twin will act as a preferential nucleation site that dictates the lateral step flow cycle.

Discussion

Our data allows us to focus on how a single twin can change the growth behavior. It is important to note that there is considerable disagreement on how twin boundaries alter the free energy for atomic layer formation. To illustrate this, the work required to form a single disc shaped nucleus on a $\{111\}$ facet, *ii* of Fig. 1b, of height given by the lattice spacing, z , and radius R^* , is $W_{\text{HOM}}^* = (\pi z \gamma_{\text{SL}}^2) / (\Omega_{\text{v}}^{\text{L}} - \Omega_{\text{v}}^{\text{S}})$, where γ_{SL} is the solid liquid (SL) interfacial energy, $\Omega_{\text{v}}^{\text{L}}$ and $\Omega_{\text{v}}^{\text{S}}$ are the bulk free energies of the liquid and solid, respectively [27]. We assume that the solid-liquid energy is isotropic to focus on the effects of the twin. If a twin boundary is present at position *iii* (Fig. 1b), then we must include the energy of the twin boundary. There will be a trijunction where the twin meets the edge of the disk with an angle ϕ , see Fig. 2b. The critical radius of curvature of the edge of the nucleus and equilibrium angle is determined by extremizing the free energy change with respect to the radius, and the angle ϕ subject to the constraint of constant nucleus volume. The latter gives the usual force balance condition at the twin solid-liquid interface trijunction, $\gamma_{\text{t}} = -2\gamma_{\text{SL}}\cos(\phi_{\text{e}})$, where ϕ_{e} is the equilibrium angle at the trijunction. Since $\gamma_{\text{SL}} > \gamma_{\text{t}}$, $\phi_{\text{e}} > 90^\circ$, the nucleus will be composed of truncated disks with the twin at the center of the two disks, Fig. 2b shows the case where $\phi < 90^\circ$. Using this shape, the reversible work for the formation of the twinned critical nucleus, defined as W_{HET}^* (where subscript HET stands for heterogeneous nucleation), is greater than that for a disk-shaped nucleus (Fig. 2a), for any $\gamma_{\text{t}} > 0$. Specifically $W_{\text{HET}}^* / W_{\text{HOM}}^* = f(\phi) = (1/\pi)[2\phi - \sin(2\phi)]$ so the presence of the twin does not, by itself, reduce the barrier for nucleation.

When nuclei are small it is well known that line or edge energies can be important during nucleation due to the small size of the nucleus, for example during the nucleation of quantum dots [28] or small liquid droplets on surfaces [29]. We thus augment the energy required to form a twinned nucleus by the line energy, γ_{l} , associated with the trijunction (region indicated by the dark orange line in Fig. 2b) where the twin in the nucleus meets the solid-liquid interfaces that compose the sides of the nucleus. We take the line energy term γ_{l} to be a function of ϕ since the bond angles between atoms are fixed, and thus the energy of the line, and hence γ_{l} , will change

with ϕ . We assume a negative line energy for $\phi < 90^\circ$. Negative line energies, unlike negative surface energies, do not lead to instabilities and lead to an atomically sharp trijunction line, unlike the case where the line energy is positive and the trijunction would be rounded [30]. Since there are two cusps on the lens shaped nucleus, the total contribution of the line energy is $2z\gamma_l(\phi)$, where z is the height of the nucleus. The importance of the energy at the nucleus edge has been noted in past literature on the formation of twinned nuclei in the Si system [11]. The expression for the free energy is extremized with respect to ϕ and R to yield the heterogeneous nucleation barrier, W_{HET}^* . The equilibrium angle at the trijunction, ϕ_e , becomes a function of $\partial\gamma_l/\partial\phi$ (see Supporting Information), and the nucleation barrier is

$$\frac{W_{\text{HET}}^*}{W_{\text{HOM}}^*} = \frac{2\gamma_l(\phi_e)}{\pi R_{\text{HOM}}^* \gamma_{\text{SL}}} + \left[\sqrt{f(\phi_e)} + \frac{f(\phi_e) \xi(\phi_e) \partial\gamma_l}{R_{\text{HOM}}^* \gamma_{\text{SL}} \partial\phi} \right]^2 \quad \text{Eqn. 1}$$

In Eqn. 1 $\xi(\phi_e) = (1/2)[\tan(\phi_e)/(\tan(\phi_e) - \phi_e)]$ and $R_{\text{HOM}}^* = \gamma_{\text{SL}}/(\Omega_v^{\text{L}} - \Omega_v^{\text{S}})$ is the radius for a critical nucleus without a twin defect. In the limit $\gamma_l = 0$, $\phi_e > 90^\circ$ the second term is greater than 1 and, as mentioned above the presence of a twin increases the energy of formation of critical nucleus above that for a twin-free nucleus. The first term is a dimensionless group that shows that R_{HOM}^* sets the length scale where the effects of the line energy becomes important, and if $\gamma_l < 0$ this term favors nucleation at a twin boundary. A reasonable estimate for γ_l is $\gamma_{\text{SL}}a$, where a is a lattice parameter [31] and thus for this term to have an effect on the nucleation process, R_{HOM}^* must be on the order of the lattice parameter.

While it is clear that a negative γ_l will favor nucleation, to illustrate quantitatively the effects of the line energy it is necessary to have an explicit function for $\gamma_l(\phi)$. Following the hypothesis that variations in $\gamma_l(\phi)$ are a consequence of the atomic bonding at the line, $\gamma_l(\phi)$ must have a small or near zero value when $\phi = 90^\circ$ where there is no cusp at the trijunction. In addition, for some angle ϕ_0 between 0° and 90° $\gamma_l(\phi) < 0$ to keep a cusp at the trijunction. Finally, $\gamma_l(\phi)$ is likely not a monotonic function since when ϕ is small, the local arrangement of atoms must be significantly different from that of the bulk lattice. This implies $\gamma_l(\phi)$ likely has a minimum value between 0° and 90° . A simple expression for $\gamma_l(\phi)$ which has these properties is $\gamma_l(\phi) = -\gamma_l^0(4/\pi)^2 \phi(\phi - \pi/2)$, where γ_l^0 is the minimum line energy value of $\gamma_l(\phi)$. Using this expression in Eqn. 1 yields a plot showing $W_{\text{HET}}^*/W_{\text{HOM}}^*$ as function of the dimensionless

parameter $\gamma_l^0/(R_{\text{HOM}}^* \gamma_{\text{SL}})$ for various ϕ_e values, see Fig. 3. Note that in Fig. 3 $R_{\text{HOM}}^* = 0.25$ nm and $\gamma_{\text{SL}} = 0.5$ J m⁻², both reasonable values for R_{HOM}^* [32], γ_{SL} [33] in NW systems.

Figure 3 shows that for progressively more negative values of γ_l^0 both the nucleation barrier ratio $W_{\text{HET}}^*/W_{\text{HOM}}^*$ and ϕ_e decrease. When $\gamma_l^0 = 0 \rightarrow \phi_e \approx 90^\circ$ and $W_{\text{HET}}^*/W_{\text{HOM}}^* \approx 1$. As $\gamma_l^0/(R_{\text{HOM}}^* \gamma_{\text{SL}})$ becomes increasingly negative, ϕ_e and $W_{\text{HET}}^*/W_{\text{HOM}}^*$ decrease. While the decrease in the energy barrier may be small, it is important to realize that small changes in the barrier can lead to orders of magnitude changes in the nucleation rate [29]. Since $W_{\text{HET}}^*/W_{\text{HOM}}^* < 1$ for realistic values of γ_l^0 and R_{HOM}^* , we propose that the line energy term at the nucleus cusp is the key parameter causing preferential nucleation along the twin plane boundary model. The actual nucleation rate will depend on factors such as the rate of atomic motion across the solid-liquid interface and the line length of the {111} facet-twin boundary trijunction [34, 35]. Our general model of nucleation along the length of *iii* (Fig. 1b) captures the essential physics of the nucleation process that allows us to rationalize all experimental NW data as well as why nuclei form at twin boundaries in bulk systems. A more detailed NW-specific nucleation model would also treat nucleation at the quadrajunction, where the twin boundary intersects the TPB, as well as consider a noncircular shape of the edge of the nucleus that is a result of anisotropic interfacial energies. The experimentally unknown configuration of the many interfaces in the TPB region, which may also include truncation facets similar to that of region *i* (Fig. 1b), however, currently does not allow the formulation of such an additional model. Such details may be not significant in the overall context given the success of our simple model. We can conclude that atomic layer nucleation along a twin defect should be favored energetically relative to a smooth planar substrate.

Conclusions

In conclusion, we establish a twin plane re-entrant based growth mechanism for catalytic NW growth. Unlike to all previously reported TPBE mechanisms, the nanoscale geometry allows steady state growth based on a *single* twin boundary. We propose that the nucleation barrier at the twin plane re-entrant groove is effectively reduced by the line energy term, and hence the twin acts as a preferential nucleation site that dictates the lateral step flow cycle that constitutes NW growth. Our results are highly relevant to controlled, selective crystal growth on the

nanoscale for a wide range of materials. Moreover, the results obtained in our NW model system provide important insights into the role of twin defects in a wide range of growth processes.

Acknowledgements

We acknowledge helpful discussions with Frances M. Ross. S. H. acknowledges funding from ERC grant InsituNANO (project number 279342). A. D. G. acknowledges funding from the Marshall Aid Commemoration Commission and the National Science Foundation. C. D. acknowledge funding from the Royal Society. P.V. acknowledges the support of ONR grant N00014-12-1-0198. We gratefully acknowledge the use of facilities within the LeRoy Eyring Center for Solid State Science at Arizona State University.

Supporting Information

Bright field ETEM video (9 frames per second, corresponding to Fig. 1) of Ge NW growing with a convex V-shaped liquid-solid interface, lattice resolved image of a twinned [112] type Ge NW, supporting crystallographic analysis and further details on Fig.1 and derivation of eqn. (1) and the non-linear equation that determines ϕ_e . This material is available free of charge via the Internet at <http://pubs.acs.org>.

References

- [1] J. W. Cahn, W. B. Hillig, and G. W. Sears, *Acta Metall.* **1964**, 12, 1421.
- [2] J. W. Faust Jr, and H. F. John, *J. Phys. Chem. Solids* **1964**, 25, 1407.
- [3] J. Cissé, H. Kerr, and G. Bolling, *Metall. Mater. Trans. B* **1974**, 5, 633.
- [4] M.-K. Kang, Y.-S. Yoo, D.-Y. Kim, and N. M. Hwang, *J. Am. Ceram. Soc.* **2000**, 83, 385.
- [5] E. Billig, and P. J. Holmes, *Acta Metall.* **1957**, 5, 53.
- [6] E. Billig, *Acta Metall.* **1957**, 5, 54.
- [7] R. S. Wagner, *Acta Metall.* **1960**, 8, 57.
- [8] A. I. Bennett, and R. L. Longini, *Phys. Rev.* **1959**, 116, 53.
- [9] D. R. Hamilton, and R. G. Seidensticker, *J. Appl. Phys.* **1960**, 31, 1165.
- [10] W. A. Tiller, *The Science of Crystallization: Microscopic Interfacial Phenomena* (Cambridge University Press, Cambridge, UK, 1991).
- [11] J.-W. Lee, U.-J. Chung, N. M. Hwang, and D.-Y. Kim, *Acta Crystallogr., Sect. A: Found. Crystallogr.* **2005**, 61, 405.
- [12] N.-b. Ming, and I. Sunagawa, *J. Cryst. Growth* **1988**, 87, 13.
- [13] J. E. Allen, E. R. Hemesath, D. E. Perea, J. L. Lensch-Falk, Z. Y. Li, F. Yin, M. H. Gass, P. Wang, A. L. Bleloch, R. E. Palmer, and L. L. Lauhon, *Nat. Nanotechnol.* **2008**, 3, 168.
- [14] E. R. Hemesath, D. K. Schreiber, E. B. Gulsoy, C. F. Kieselowski, A. K. Petford-Long, P. W. Voorhees, and L. J. Lauhon, *Nano Lett.* **2012**, 12, 167.
- [15] Disclaimer: The full description of the procedures used in this paper requires the identification of certain commercial products and their suppliers. The inclusion of such information should in no way be construed as indicating that such products or suppliers are endorsed by NIST or are recommended by NIST or that they are necessarily the best materials, instruments, software or suppliers for the purposes described.
- [16] A. D. Gamalski, C. Ducati, and S. Hofmann, *J. Phys. Chem. C* **2011**, 115, 4413.
- [17] A. D. Gamalski, J. Tersoff, R. Sharma, C. Ducati, and S. Hofmann, *Nano Lett.* **2010**, 10, 2972.
- [18] S. A. Dayeh, J. Wang, N. Li, J. Y. Huang, A. V. Gin, and S. T. Picraux, *Nano Lett.* **2011**, 11, 4200.
- [19] R. Boukhicha, L. Vincent, C. Renard, C. Gardès, V. Yam, F. Fossard, G. Patriarche, F. Jabeen, and D. Bouchier, *Thin Solid Films* **2012**, 520, 3304.
- [20] C. Cayron, M. Den Hertog, L. Latu-Romain, C. Mouchet, C. Secouard, J.-L. Rouviere, E. Rouviere, J.-P. Simonato, *J. Appl. Cryst.* **2009**, 42, 242.
- [21] F. J. Lopez, E. R. Hemesath, L. J. Lauhon, *Nano Lett.* **2009**, 9, 2774.
- [22] K. W. Schwarz, and J. Tersoff, *Nano Lett.* **2012**, 12, 1329.
- [23] D. B. Williams, and C. B. Carter, *Transmission electron microscopy: a textbook for materials science* (Springer, New York, NY, 1996).
- [24] A. A. Stekolnikov, and F. Bechstedt, *Phys. Rev. B* **2005**, 72, 125326.
- [25] C. Y. Wen, J. Tersoff, K. Hillerich, M. C. Reuter, J. H. Park, S. Kodambaka, E. A. Stach, and F. M. Ross, *Phys. Rev. Lett.* **2011**, 107, 025503.
- [26] Y. Wu, Y. Cui, L. Huynh, C. J. Barrelet, D. C. Bell, and C. M. Lieber, *Nano Lett.* **2004**, 4, 433.
- [27] D. A. Porter, K. E. Easterling, and M. Y. Sherif, *Phase Transformations in Metals and Alloys* (CRC Press, Boca Raton, FL, 2009).
- [28] V. A. Shchukin, and D. Bimberg, *Rev. Mod. Phys.* **1999**, 71, 1125.

- [29] K. F. Kelong, and A. L. Greer, *Nucleation in Condensed Matter* (Elsevier, Amsterdam, The Netherlands, 2010).
- [30] J. W. Gibbs, *American Journal of Science and Arts* **1878**, 16, 441.
- [31] C. M. Retford, M. Asta, M. J. Miksis, P. W. Voorhees, and E. B. Webb, III, *Phys. Rev. B* **2007**, 75, 075311.
- [32] F. Glas, J.-C. Harmand, and G. Patriarche, *Phys. Rev. Lett.* **2007**, 99, 146101.
- [33] J. Kim, J. Tersoff, C. Y. Wen, M. C. Reuter, E. A. Stach, and F. M. Ross, *Phys. Rev. Lett.* **2009**, 103, 155701.
- [34] V.G. Dubrovskii, N.V. Sibirev, J.C. Harmand and F. Glas, *Phys. Rev. B* **2008**, 78, 235301.
- [35] J.W. Cahn, *Acta Metall.* **1956**, 4, 449.

Figures

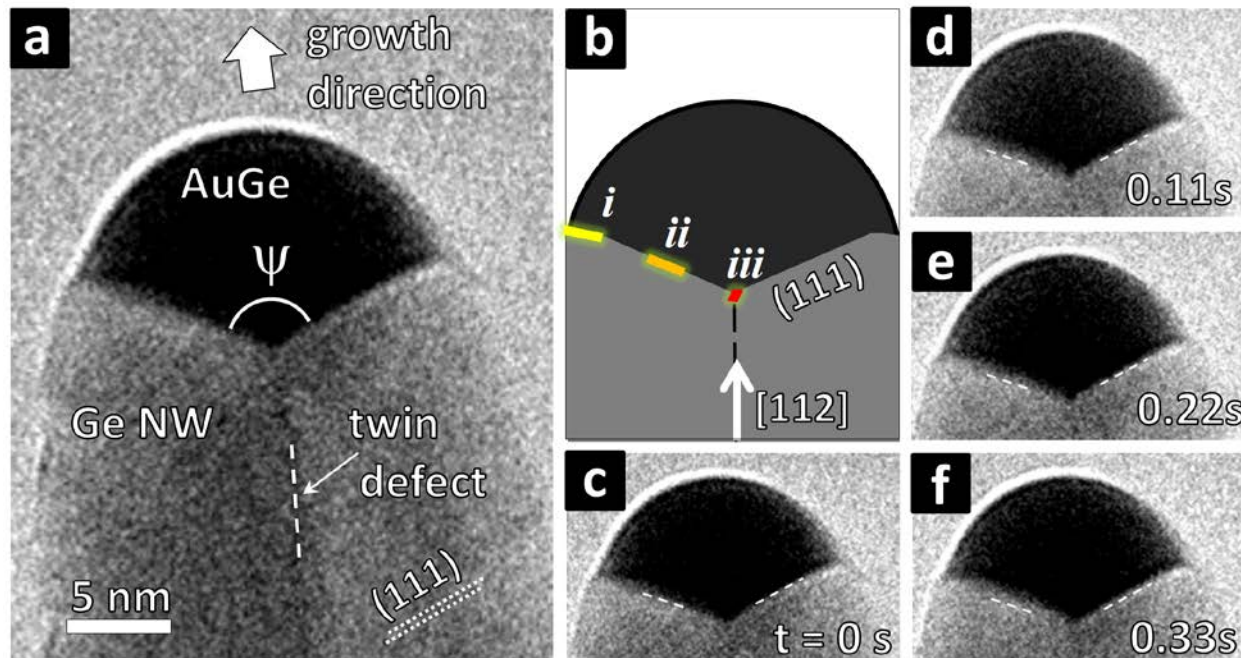


Figure 1: (a) Twinned V-shaped interface in a [112] type Ge NW growing from a liquid catalyst in 0.64 Pa total pressure of Ge_2H_6 (30 % mole fraction in He) at 341 °C. The angle ψ measures $\approx 131 \pm 2^\circ$. (b) Schematic diagram of the twinned NW. At the liquid-solid interface three regions are identified: *i* corresponds to the TPB region which connects to the (111) facets, *ii* is the flat (111) facet, *iii* indicates the basin of the twin boundary. (c-f) Sequence of successive frames in the growth video [see Supporting Information, Video V1]. Dashed lines in (c) are guides to the eye to mark the approximate projected position of the liquid-solid interface, and are reproduced for reference at the same position in frames d-f.

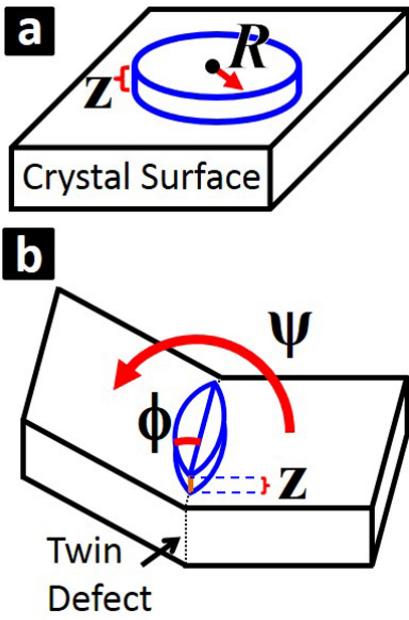


Figure 2: (a) Cylindrical 2D nucleus of height z and radius R on a smooth planar substrate. (b) A lens shaped 2D nucleus of height z with the same radius of curvature as the cylindrical nucleus in (a). The angle ϕ determines the contact angle of the nucleus relative to the twin plane.

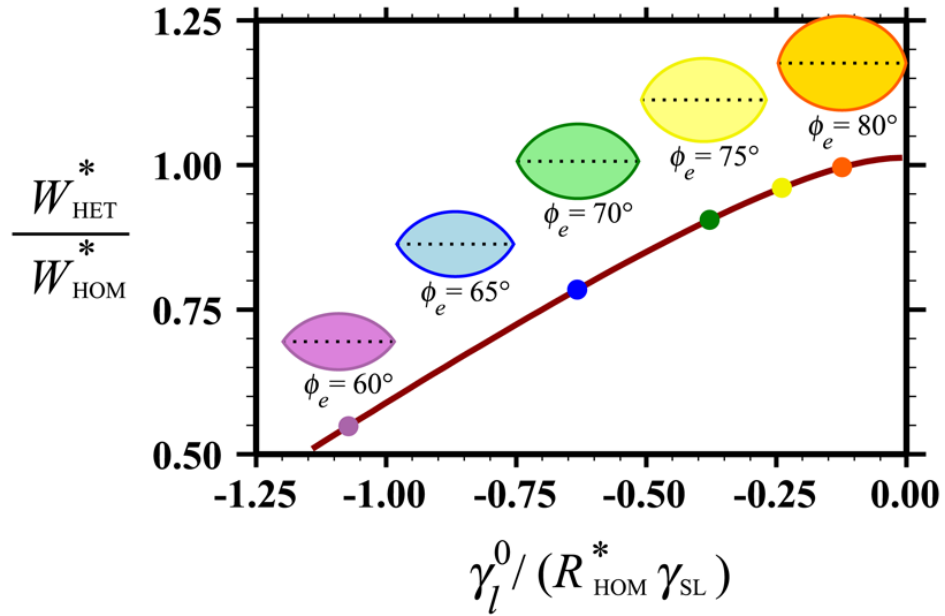


Figure 3: Plot of $W_{\text{HET}}^* / W_{\text{HOM}}^*$, representing the ratio of heterogeneous to homogeneous nucleation barriers. For each of the colored points a top view of the nucleus' area is given along with the equilibrium angle ϕ_e . The black dashed line indicates the location of the twin defect running through each nucleus.

Table of Contents Figure

